

Article

Weatherability of Bamboo Scrimber: Enhance in Photostability of Substrate and Coatings

Yang Yang ^{1,2,3,†}, Lei Zhang ^{1,4,†}, Hongfei Huo ^{1,3}, Minzhen Bao ², Zaixing Wu ², Yongjie Bao ², Yuhe Chen ², Zhongfeng Zhang ^{1,3,5,*} and Neng Li ^{2,*}

¹ College of Furniture and Art Design, Central South University of Forestry and Technology, Changsha 410000, China; yang193829@163.com (Y.Y.); loneyanzi1990@163.com (L.Z.); 15320201468@163.com (H.H.)

² Key Laboratory of High Efficient Processing of Bamboo of Zhejiang Province, China National Bamboo Research Center, Wenyi Road 310, Hangzhou 310012, China; baominzhen@zstu.edu.cn (M.B.); jwu002@126.com (Z.W.); baoyongjie@caf.ac.cn (Y.B.); chenyuhe@caf.ac.cn (Y.C.)

³ Green Furniture Engineering Technology Research Center, National Forestry and Grassland Administration, Changsha 410000, China

⁴ Dongyang Furniture Institute, Dongyang 322100, China

⁵ Hebei Mu Huai Smart Home Co., Ltd., Handan 057650, China

* Correspondence: csfuzzf@163.com (Z.Z.); lineng@caf.ac.cn (N.L.)

† These authors contributed equally to this work.

Abstract: Enhancing the weatherability of bamboo-based products is essential for increasing their application lifespan. In this study, a composite protective coating containing organic and inorganic UV absorbers and a hindered amine light stabilizer (HALS) was investigated for outdoor bamboo scrimber (OBS). The optical properties of weathered coated and uncoated samples were investigated by colorimetry and UV-Vis spectrophotometry. Fourier transform infrared spectroscopy (FTIR), X-ray photoelectron spectroscopy (XPS), and thermal gravimetric analysis (TGA) were used to determine the physicochemical properties of the coating. The addition of HALS improved the photostability of the coating and preserved the properties of OBS. Compared to resin-coated samples, alicyclic amines in HALS inhibit photooxidation reactions between bamboo lignin and the coating adhesive. This inhibition is critical for maintaining the UV-shielding performance of the coating. We have developed a photostable protective coating for bamboo-based products whose widespread use can significantly help conserve critical forest resources.

Keywords: stereoscopic protective coating; outdoor bamboo scrimber; photo-stabilizer; weatherability



Citation: Yang, Y.; Zhang, L.; Huo, H.; Bao, M.; Wu, Z.; Bao, Y.; Chen, Y.; Li, N.; Zhang, Z. Weatherability of Bamboo Scrimber: Enhance in Photostability of Substrate and Coatings. *Forests* **2022**, *13*, 467. <https://doi.org/10.3390/f13030467>

Received: 22 February 2022

Accepted: 14 March 2022

Published: 17 March 2022

Publisher's Note: MDPI stays neutral with regard to jurisdictional claims in published maps and institutional affiliations.



Copyright: © 2022 by the authors. Licensee MDPI, Basel, Switzerland. This article is an open access article distributed under the terms and conditions of the Creative Commons Attribution (CC BY) license (<https://creativecommons.org/licenses/by/4.0/>).

1. Introduction

Bamboo is a widely used sustainable building and construction material possessing an attractive natural color and beautiful texture. Bamboo has a high strength-to-weight ratio and can be processed easily [1–3]. Bamboo is abundant and cultivated in different regions around the world. In particular, bamboo plantations comprise around 32 million hectares in total with 4 million hectares in China [4]. Bamboo scrimber is one of the main bamboo products and is obtained by crushing bamboo culm into fibers and pressing them into the required shape. However, when bamboo scrimber is used outdoors, environmental factors, such as solar radiation, moisture, oxygen, and high temperature cause discoloration and loss of glossiness [5,6]. Furthermore, weathering causes bamboo scrimber to lose strength, split, become rough, and exhibit chalking [7]. Solar radiation, specifically ultraviolet (UV) radiation, is the main contributor to the degradation process (Figure 1) [8–10]. Therefore, it is essential to develop UV-radiation-resistant coatings for outdoor bamboo scrimbers (OBSs).

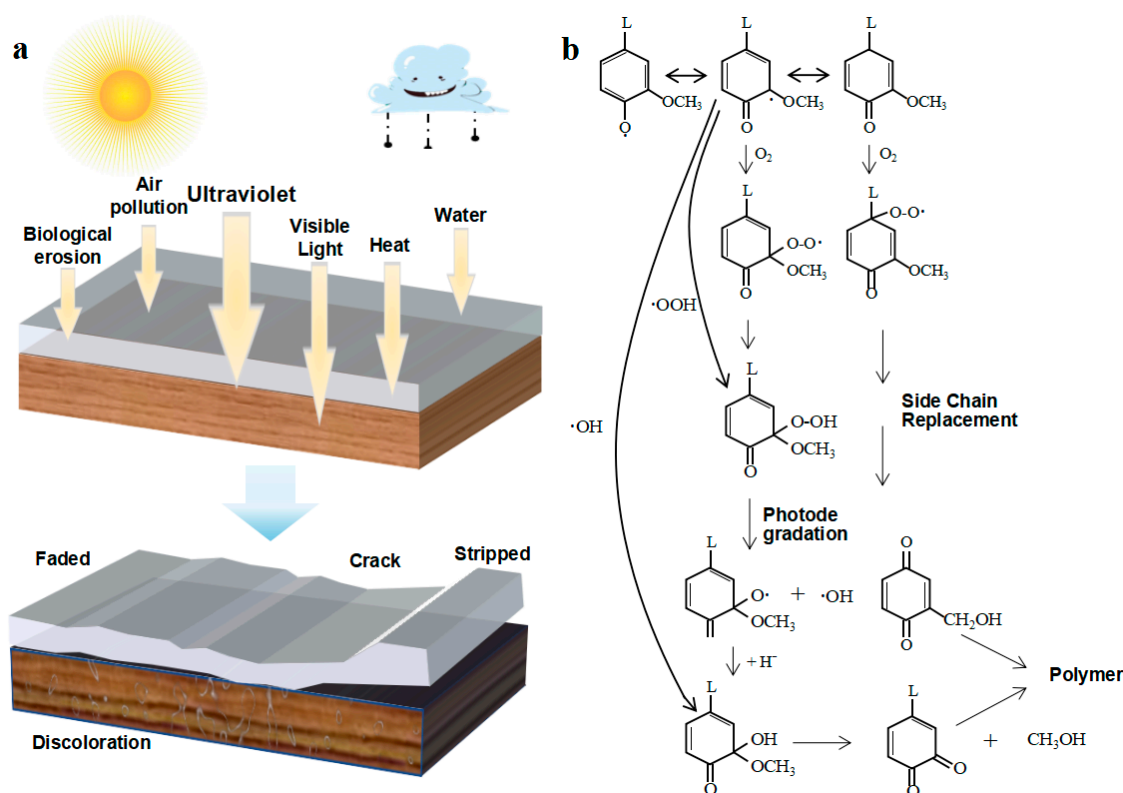


Figure 1. (a) The factors affecting wood and coating degradation; (b) α -Quinone and β -quinone forming from initial phenoxy radical.

In order to improve the weathering durability of wooden furniture, various methods for protecting wood against weathering are applied. The main methods for mitigating the adverse effects of the outdoor environment include wood modification and protection with coatings. Thermal modification and chemical modification are common methods of wood modification. Thermal modification is the controlled process of heating the wood with a maximum temperature of 250 °C under an oxygen free atmosphere [11]. Thermal modification is a commercialized technique for increasing the biological durability and dimensional stability of wood, but it cannot adequately protect the wood from the weathering effect when it was exposed outdoors for a long time [12–14]. Chemical modification of wood is defined as a chemical reaction between the wood polymeric constituents (mainly hydroxyl groups) and chemical reagent, resulting in the formation of a covalent bond between the reagent and wood substrate, so as to improve the dimensional stability, anti-corrosion ability, or other properties of wood [15,16]. The most common methods of chemical modification are esterification and etherification of hydroxyl groups in the cell wall, and the commonly used chemicals are anhydrides, acid chlorides, alkyl halogenides and epoxides [17]. Among various wood chemical modifications, acetylation has been the most studied [18]. Nevertheless, It has been established that acetylation is not very effective at protecting wood from photodegradation [19,20]. That is because the deacetylation of the wood surface occurs, resulting in the photoprotective effect of acetylation being lost with prolonged exposure of the acetylated wood to the weather [19]. Wood modification is usually used in combination with coating because of the higher dimensional stability of modification wood, which reduces the stresses in the coating that originate from the dimensional changes of the substrate [21,22].

The common way to protect wood from weathering is to protect it with a wide range of coatings, such as treatment with opaque paint or coatings containing UV absorbers. Coating a wood substrate with opaque paint can efficiently block UV radiation and reduce photodegradation. However, opaque paint covers the beautiful textures of bamboo and

wood. Therefore, opaque paint is rarely used as a coating. Organic and inorganic UV absorbers are effective additives for minimizing the photodegradation of outdoor bamboo and wood products. Inorganic UV absorbers are mainly nano-metal oxides, such as nano-ZnO, TiO₂, and SiO₂ [23–25]. Impregnating the coating with a nanoparticle suspension can significantly improve the photostability of bamboo and preserve aesthetic properties, such as color and gloss during photoweathering and resin-based coatings prepared with an inorganic UV absorber have strong surface adhesion [26,27]. Organic UV absorbers are widely used in the surface treatment of plastics, wood, and other materials [28,29]. Organic UV absorbers mainly include benzotriazole, salicylic acid, and benzophenone which all contain hydroxyl groups. Hydroxyl groups convert UV absorption into heat energy by forming stable hydrogen bonds and hydrogen bond chelating rings [30]. Inorganic UV absorbers have antibacterial properties and strong antileachability, while organic UV absorbers are simple to process, low cost, and have high visible light penetration [31,32]. However, inorganic and organic UV absorbers have certain disadvantages that limit their widespread application to bamboo and wood [33]. Inorganic UV absorbers rely on the nanometer size effect and are difficult to disperse in solution, with the nanoparticles tending to aggregate. Moreover, inorganic nanoparticle UV absorbers are very expensive. By contrast, organic UV absorbers leach easily due to their small molecular weight and their inability to form chemical bonds with film-forming materials. Furthermore, the thermal stability of organic UV absorbents is relatively poor. The UV shield-coated UV absorbent has excellent UV shielding performance and can effectively delay weathering, improving the service life of the substrate. However, the carriers of UV absorbents are usually water-based or oil-based film-forming matter (resins) and the UV shield coating can also absorb UV light, thus resulting in photodegradation. Surface coatings are prone to cracking after photodegradation, allowing water and oxygen to enter the interface between the coating and the substrate, leading to a rapid decline in the film coating adhesion with the substrate followed by cracking and peeling [31,34]. Peeling of the surface coating fully exposes the bamboo substrate to UV radiation, ruining the aesthetics of the bamboo and reducing its service life.

Hindered amine light stabilizers (HALS) are widely used in the plastics and textile industries. Hindered amines can capture free radicals, decompose hydrogen peroxide, and transfer the energy of the excited state molecules to reduce photodegradation reactions. Therefore, the addition of HALS into coatings for bamboo and wood should be explored.

In this study, inorganic UV absorber, organic UV absorber, HALS, and acrylic resin were combined to develop a stereoscopic protective coating for OBS. We hypothesized that the stereoscopic protective coating improves the photostability of bamboo substrates by shielding UV radiation and enhancing the weatherability of coatings through the absorption of free radicals and inhibition of photodegradation reactions by HALS. A weathering test box was used to simulate the outdoor environment. The optical properties of the samples were investigated by determining the color parameters and by UV-Vis measurements. Changes in the functional groups in the coatings after UV exposure were examined using Fourier transform attenuated total reflection infrared spectroscopy (FTIR-ATR). The molecular structure and valence states of the coatings were characterized by X-ray photoelectron spectroscopy (XPS) and the thermochemical properties of the coatings were evaluated by thermogravimetric analysis (TGA).

2. Materials and Methods

2.1. Preparation of Outdoor Bamboo Scrimber and Coatings

Moso bamboo (*Phyllostachys pubescens* Mazel): 4-year-old, collected from Anji County, Zhejiang Province.

Low molecular weight phenolic resin (PF): solid content 47.91%, viscosity 35 CPS (30 °C), pH 10~11.

Four-year-old moso bamboo culms were used as raw materials to make OBS. First, raw bamboo was processed into an oriented bamboo-fiber mat (OBFM). Following this, the

OBFMs were air-dried till their moisture content (MC) was approximately 6.97 wt% and immersed in 30 wt% PF resin solution for approximately 6 min at 25 °C. Subsequently, they were drip-dried for 2 to 3 min and weighed to ensure that the final PF resin content was approximately 15 wt%. The resin-impregnated OBFMs were then air-dried to obtain an MC of approximately 12 wt%. Finally, the OBS material was created by assembling mats symmetrically along the grain in a mold and hot pressed (CARVER 3353, Mascatine, IA, USA) at 145 °C for a time equivalent to 0.5 min/mm. The resin content of the prepared OBS was 14%, and the density was 1.10 g/cm³. Prior to the application of the paint, the OBS was cut into 70 mm × 20 mm × 1.5 mm pieces after conditioning in a room with constant temperature and humidity for 2 weeks. Subsequently, the surface of the OBS was sanded down using abrasive paper to achieve a uniform thickness surface.

Acrylic acid, siban (sorbitan palmitate), Tween (polyoxyethylene dehydrated sorbitol monooleate), and cyclohexan were used to prepare the clear-coat resin (Table 1). Siban and tween were used as dispersants and surfactants for the dispersion of subsequent additions of NZnO. Acrylic acid is an excellent film-forming material for outdoor applications because of its good weatherability. The coating formulations are presented in Table 2.

Table 1. Clear-coat resin.

Additives	Supplier	wt%
Acrylic acid	Saisili	86.20
Siban	Macklin	2.30
Tween	Macklin	2.30
Cyclohexan	Chronchem	9.20

Table 2. Formulations of coatings.

Samples	Additives (%)						Total(%)
	BTZ-1	NZnO	HA1	HA2	Clear-Coat Resin	Ethanol	
CS	0.00	0.00	0.00	0.00	87.00	13.00	100.00
HC1	0.00	0.00	2.00	0.00	87.00	11.00	100.00
HC2	0.00	0.00	0.00	2.00	87.00	11.00	100.00
BZC	2.00	3.50	0.00	0.00	87.00	7.50	100.00
BZHC1	2.00	3.50	2.00	0.00	87.00	5.50	100.00
BZHC2	2.00	3.50	0.00	2.00	87.00	5.50	100.00

BTZ-1 (benzotriazole), NZnO, hindered amine, and ethanol act as organic UV absorbers, inorganic UV absorbers, light stabilizers, and diluters, respectively. The control sample (CS) was made up of clear-coat resin and ethanol without the addition of a UV absorber and HALS. HC1 and HC2 are composed of HA1 (bis(2,2,6,6-tetramethyl-1-(octyloxy)-4-piperidinyl) ester) and HA2 (methyl (1,2,2,6,6-pentamethyl-4-piperidinyl) sebacate) with clear-coat resin, respectively. The NZnO dispersed by siban and Tween was added to the coating with BTZ-1 to prepare a coating of BZC which was an inorganic and organic hybrid coating. The protective coatings BZHC1 and BZHC2 were composed of BTZ-1, NZnO, HA1/HA2, ethanol, and clear-coating resin.

2.2. Preparation of Free Films and Coating of OBS

Quartz glass with dimensions of 45 mm × 12.5 mm × 1.2 mm were used as substrates for free film preparation. The coatings shown in Table 1 were applied to quartz glass slides with a dry film mass of 5.00 ± 0.40 mg. Prior to coating, the formulations were stirred for 8 min using a magnetic stirrer (78HW-1). Next, the slides were coated at a temperature of 20 °C and allowed to rest until most of the air bubbles were eliminated; this took approximately 20 min. The resulting free films were dried in air at 20 °C for 24 h.

They were then heated at 135 °C for 2 h to accelerate the curing of the acrylic resin prior to analysis [35].

OBS samples with dimensions of 70 mm × 20 mm × 1.5 mm were coated with free films (Figure 2). The OBS samples coated with free films CS, HC1, HC2, BTC, BZHC1, and BZHC2 are denoted as CS-B, HC1-B, HC2-B, BTC-B, BZHC1-B, and BZHC2-B, respectively.

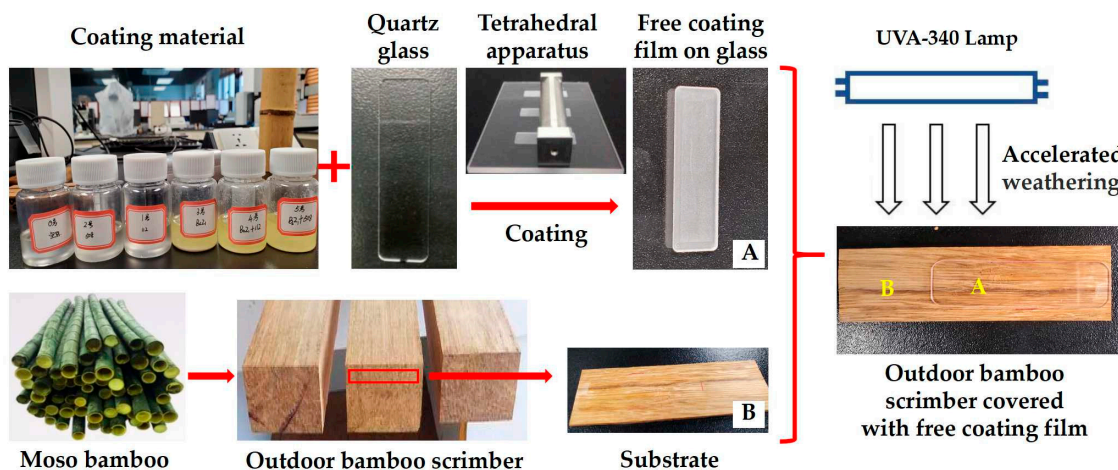


Figure 2. Preparation of weatherability OBSs coated with free films.

2.3. Artificial Accelerated Weathering

Accelerated weathering experiments were performed in a UV weathering test box (ZN-P, Hangzhou Nine Ring Fu Da Industrial Co., Ltd., Hangzhou, China) according to ASTM G154-16 [36]. Samples were fixed in stainless steel holders and cyclically exposed to UV radiation at a black panel temperature of 63 °C for 8 h and condensation at a black panel temperature of 50 °C for 4 h. The UV radiation intensity was 25 W/m² (UVA-340 lamp). The sample was characterized after 50, 100, 150, 200, 250, and 300 h exposure.

2.4. Color Measurement and Calculation of Inhibition Rate of Photo Decolorization

The surface colors of the OBS substrate during weathering were measured using a colorimeter (CM-3600d, Konica Minolta Inc., Kyoto, Japan). Nine replicate measurements were performed on the defined points on the sample surfaces. The color parameters L^* , a^* , and b^* of the CIELAB color system were measured according to ASTM D 2244-07 [37]. L^* , a^* , and b^* represent the indices of lightness, red and green, yellow, and blue, respectively. The overall color modulus difference (ΔE), which represents the change in color, was calculated by Equation (1):

$$\Delta E = \sqrt{(L_1^* - L_0^*)^2 + (a_1^* - a_0^*)^2 + (b_1^* - b_0^*)^2} \quad (1)$$

where L_0^* , a_0^* , and b_0^* , and L_1^* , a_1^* , and b_1^* are the color parameters of the samples before and during weathering, respectively.

2.5. UV-Vis Spectroscopy Analysis

The UV spectra of the free films were recorded using a UV-Vis spectrophotometer (UV-2401 PC, Kyoto, Japan). Quartz slides were sized to exactly fit the sample cell of the spectrophotometer, and spectra were recorded at wavelengths of 200–800 nm in increments of 1 nm at moderate scanning speed.

2.6. Fourier Transform Infrared Spectroscopy Analysis

FTIR-attenuated total reflectance (ATR) spectroscopy of free films on quartz glass was carried out using a Nicolet iS10 spectrophotometer (Thermo Scientific, Waltham, MA, USA) equipped with a diamond crystal ATR accessory (Smart iTX, Thermo Scientific, USA). The resolution was set at 4 cm⁻¹, and 64 scans were recorded for each analysis with a scanning

range of 400 cm^{-1} to 4000 cm^{-1} . Three measurements were performed on each free film sample on different spots [30].

2.7. X-ray Photoelectron Spectroscopy Analysis

XPS was performed on a Kratos Axis Ultra spectrometer (Kratos Analytical Ltd., Manchester, UK) using a monochromatic Al K α X-ray source ($h\nu = 1486.6\text{ eV}$) with a power of 300 W and a take-off angle of 308° relative to the sample surface. The measurements were performed under a high vacuum of 5×10^{-10} mbar at room temperature. The investigated area was typically $9 \times 9\text{ mm}^2$. The core-level binding energies (BEs) were aligned with the C1s peak binding energy (BE) peak (284.60 eV). Data were analyzed using Peakfit software. The atomic C/O ratios were calculated from the C1s and O1s peak areas.

2.8. Thermogravimetry Analysis

TGA was conducted on the free films using a thermogravimetric analyzer (TGA 1, STARe System, Mettler-Toledo, Columbus, OH, USA) which allows for the simultaneous detection of mass changes and heat effects of decomposition. All samples were performed under a dry and pure nitrogen atmosphere with a flow rate of $50\text{ mL}\cdot\text{min}^{-1}$ and at a temperature range of $25\text{--}800\text{ }^\circ\text{C}$ at a heating rate of $10\text{ }^\circ\text{C}\cdot\text{min}^{-1}$.

3. Results and Discussion

3.1. Color Analysis of OBS Substrate

The color changes in OBS are related to chemical changes, such as the degradation of bamboo lignin. The color changes in response to UV irradiation of the surfaces of the OBS coated with different films are shown in Figure 3. UV exposure has a great influence on the color of CS-B, HC1-B, and HC2-B, and it has an obvious darkening tendency (Figure 3a), reddening (Figure 3b), yellowing (Figure 3c), and the total color difference increased (Figure 3d). The colorimetric parameter L^* (lightness) of all samples shows a decreasing tendency with the extension of irradiation time, indicating that UV exposure leads to the gradual darkening of the OBS surface [38]. The largest change in L^* after 300 h of weathering was observed in sample CS-B (-14.42) without coating, followed by samples HC2-B (-13.94) and HC1-B (-12.67). These results suggest that the lightness of OBS without protection is susceptible to photodegradation and coating with a light stabilizer alone cannot significantly improve the lightness stability of OBS. The smallest changes in L^* were obtained by sample BZHC1-B (-2.01), followed by BZHC2-B (-3.17) and BZC-B (-5.54). This indicates that the stereoscopic protective coatings were successful in promoting the lightness stability of OBS. Both BZHC1-B and BZHC2-B exhibited better performance in L^* stability than BZC-B after exposure. The combined application of UV absorber and HALS promoted the lightness stability of OBS.

The Δa^* value of samples CS-B, HC1-B and HC2-B increased sharply (towards reddening) in the first 100 h of exposure and slowed down considerably after this stage. The Δa^* value of samples CS-B, HC1-B and HC2-B after 300 h weathering were 4.08, 4.59 and 3.80, respectively. The tendency of samples CS-B, HC1-B and HC2-B to redden was attributed to the production of a large number of adjacent quinone groups during weathering [39,40]. The smallest Δa^* was observed in sample BZHC1-B (0.48); samples BZC-B and BZHC2-B also showed good stability in a^* , with Δa^* values of 1.54 and 0.63, respectively. These results illustrate the effectiveness of the stereoscopic protective coatings in preserving the a^* color parameter of the substrate.

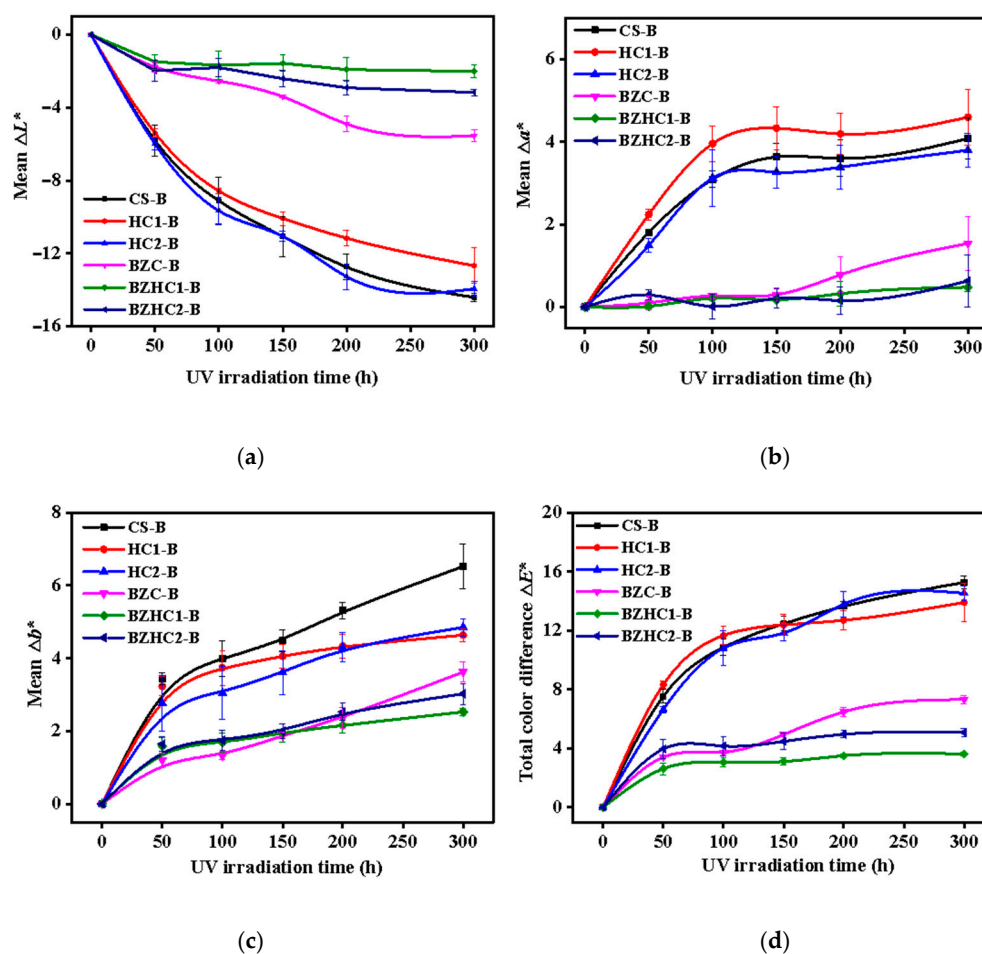


Figure 3. Changes of L^* , a^* , b^* and ΔE^* of OBS during weathering.

All samples showed an obvious increase in the colorimetric parameter b^* after exposure. Sample CS-B showed the greatest change in b^* (towards yellow) with a Δb^* of 6.52 [41]. Samples HC2-B and HC1-B had Δb^* of 4.85 and 4.63, respectively. Similar to the results for ΔL^* and Δa^* , the sample of BZHC1-B with stereoscopic protective coating exhibited the best stability in b^* and its Δb^* was only 2.52, which is approximately 38.65% of the Δb^* of CS-B.

The ΔE^* values, reflecting the overall color change of the samples after exposure, are presented in Figure 3d. The ΔE^* of samples CS-B, HC1-B, and HC2-B showed a rapid increase in the first 100 h of exposure and continued to increase in the next 200 h of exposure. The largest ΔE^* was obtained by sample CS-B (15.26) after 300 h of weathering, followed by samples HC1-B (13.92) and HC2-B (14.54). This indicates that the surface of the OBS substrate underwent a large number of photochemical reactions and consequently, a large number of chromophoric groups were produced during photodegradation [42]. The poor color stability of samples HC1-B and HC2-B confirmed that light stabilizers alone cannot adequately protect the substrate color [43]. The ΔE^* of sample BZC-B was 7.32 after 300 h of weathering, which was less than half of the ΔE^* value of CS-B. This illustrates that the coating consisting of inorganic and organic UV absorbers weakened the photochromic reaction through UV shielding. Much better photostability against color change was obtained by samples covered with stereoscopic protective coatings; the ΔE^* values of samples BZHC1-B and BZHC2-B were 3.62 and 5.09, respectively. This result was similar for ΔL^* , Δa^* , and Δb^* , and the smallest changes for BZHC1 illustrate that the coating containing both UV absorber and HALS has provided the best photostability protection for OBS.

Photos of the blank sample without exposure and weathered samples are presented in Figure 4. The covered area is the area between the red dashed lines, and the intuitive presentation results are consistent with the colorimetric parameter investigation. The photochromism of sample CS-B was remarkable, and there was no obvious boundary between the covered and uncovered areas. The photochromism of samples HC1-B and HC2-B was more pronounced than that of the blank sample. However, the covered area of BZC-B, BZHC1-B, and BZHC2-B exhibited good behavior after exposure, and a noticeable difference was observed between the covered and exposed areas.

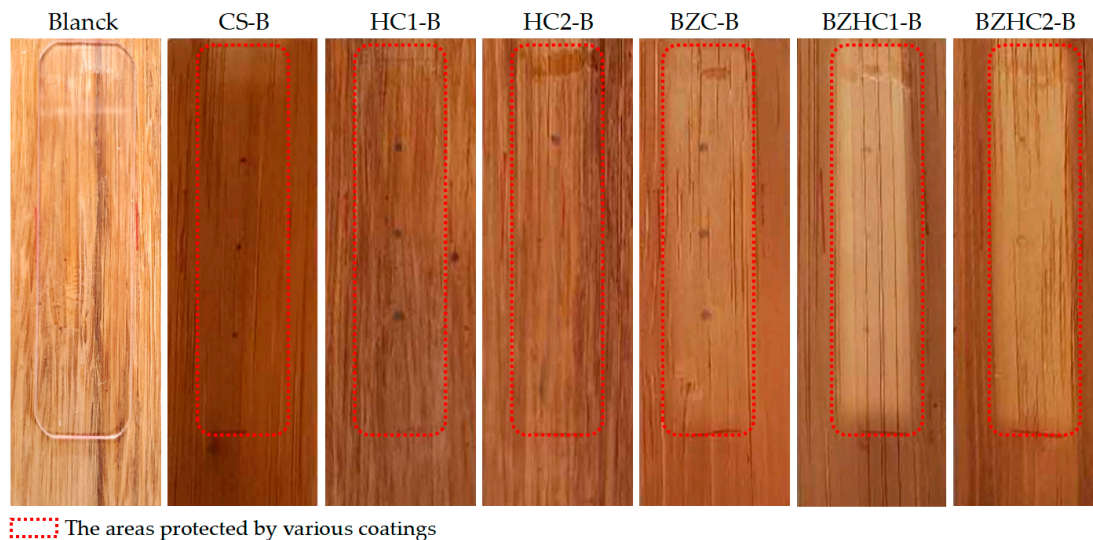


Figure 4. The pictures of Blank sample without exposure and weathered samples (300 h of exposure).

3.2. UV-Vis Analysis of Free Films

Figure 5 shows the UV-Vis spectra of free films after exposure which were used to evaluate the changes in the UV shielding performance of free films during weathering. All curves exhibited lower absorbance in the visible light region and higher absorbance in the UV light region. The UV absorption of samples CS, HC1 and HC2 were stable in the 200–280 nm range. The absorption peak of acrylic resin appeared at 258 nm, indicating that it is useless for the anti-photodegradation of outdoor wood and bamboo [44]. Samples BZC, BZHC1, and BZHC2 also showed stronger UV absorption in the 280–400 nm region, and two obvious absorption peaks appeared at 312 nm and 354 nm, indicating that the free films provided effective UV shielding for the substrate [45]. The UV absorbance of all samples showed a decreasing tendency with the extension of irradiation time, suggesting that the chemical structure of free films could be destroyed by exposure to UV, resulting in the loss of UV shielding capability. The UV absorbance values of samples CS (1.33), HC1 (1.38), and HC2 (1.22) at 258 nm were slightly different before exposure, indicating that the addition of HALS did not significantly improve the UV shielding performance of the coating. The highest UV absorbance values at 312 nm and 354 nm without weathering were observed in samples BZC (2.17, 2.29), followed by BZHC2 (2.08, 2.22) and BZHC1 (2.03, 2.17). The BZC sample also showed the greatest change in UV absorbance values at 312 nm (−0.87) and 354 nm (−0.90) after 300 h of weathering, and the peak absorbance values decreased by 59.90% and 60.00%, respectively. This indicates that the UV absorber (BTZ) was easily degraded and lost its ability to absorb UV light during weathering. However, the loss rate of UV light absorbance values of free films was reduced after the addition of HALS, and the peak absorbance values of the BZHC1 and BZHC2 samples decreased by 32.40% and 33.20% (peak at 312 nm) and 46.70% and 47.30% (peak at 354 nm), respectively, after weathering. This verifies that the stereoscopic protective coating with added HALS improved the stability of the UV shielding. HALS absorbed free radicals and interrupted the photodegradation reactions in the free film [46].

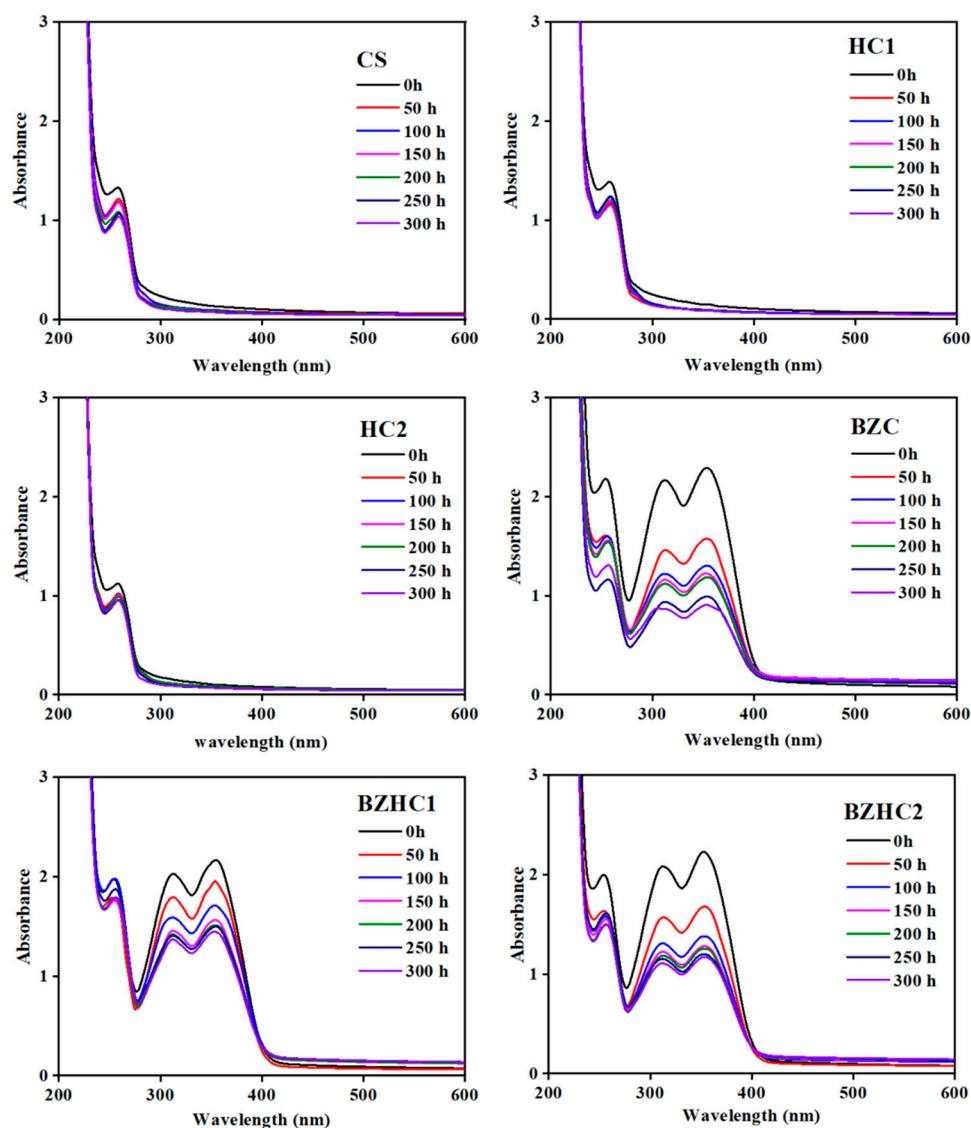


Figure 5. UV-Vis spectrum of free films during weathering.

3.3. FTIR-ATR Analysis of Free Films

FTIR-ATR spectroscopy was used to investigate the changes in the functional groups of the coatings during weathering and the photodegradation products of the samples exposed to UV radiation. The FTIR-ATR spectra of the free films before and after weathering are presented in Figure 6. The relative intensities of the absorption peaks were calculated and are listed in Table 3. The absorption peak at 1453 cm^{-1} is attributed to the stretching of $\text{C}=\text{C}$ bonds, whose intensities were steady after exposure due to their greater binding energy compared to other units. Therefore, the peak at 1453 cm^{-1} was used as a baseline reference. The intensity of the peak at 1730 cm^{-1} relative to that at 1453 cm^{-1} (I_{1730}/I_{1453}) for all samples showed an increasing tendency after weathering, which indicates an increase in $\text{C}=\text{O}$ stretching in conjugated aryl ketones and reveals that the samples undergo various degrees of photooxidation during exposure to UV radiation [26]. The relative intensity of the peak at 1730 cm^{-1} of sample CS progressively increased after exposure, and the increase in sample CS (76.77%) was the largest followed by samples HC1 and HC2, with values of 73.53%, and 69.23%, respectively. These results indicate that the free films without protection were easily photo oxidized, and the addition of HALS slightly decreased the speed of photooxidation compared with sample CS [47]. The increased proportions of the free film after weathering were obviously observed in the BZC, BZHC1, and HZHC2

samples; the proportion of BZHC1 was the smallest (20.98%), followed by BZHC2 (32.06%). This suggests that stereoscopic protective coatings provide better protection from photooxidation than other coatings [48]. An increase in the relative intensity of the absorption peaks at 1164 cm^{-1} and 1071 cm^{-1} were observed after exposure, which was attributed to the conjugated ester-based C=O stretching vibration and C–O deformation in secondary alcohols and aliphatic ethers, respectively. The increased proportion of sample BZHC1 was only 4.81% and 1.59%, which was the smallest value at the peak of 1164 cm^{-1} and the second smallest value at the peak of 1071 cm^{-1} in all samples. This confirmed the photooxidation of samples during exposure and the role of stereoscopic protective coatings in the reduction of photooxidation. The relative intensities of 1602 cm^{-1} and 1382 cm^{-1} peaks were comparatively stable compared with other peaks during weathering, probably because of the higher binding energy of aromatic and skeletal C–H bonds. The relatively high intensity of the peak at 991 cm^{-1} , which is attributed to the C–H bending vibration showed a decreasing tendency after exposure, and the decrease in the degree of protection by the coatings was relatively small, implying that stereoscopic protective coatings improved the photodegradation resistance of free films [49].

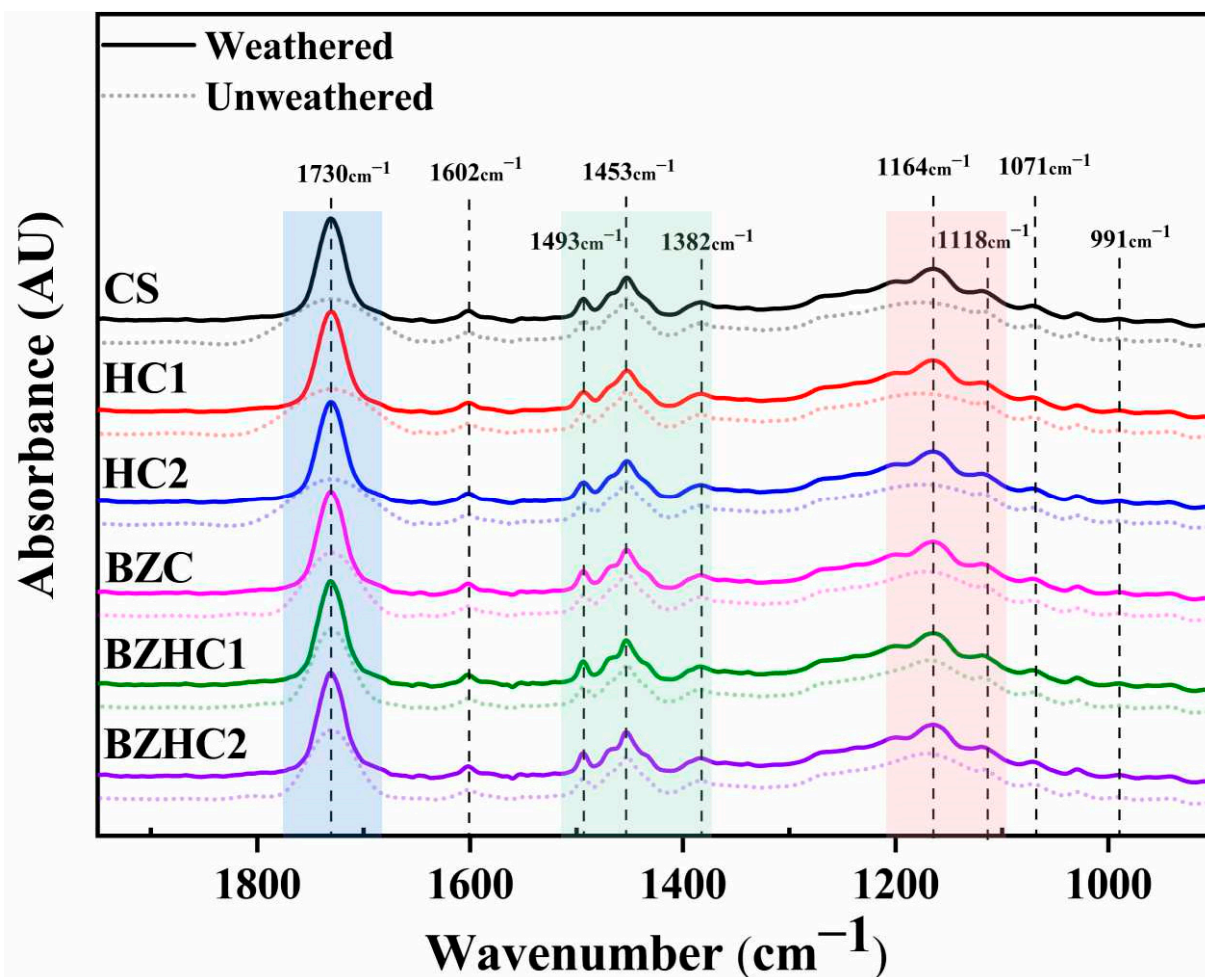


Figure 6. FTIR-ATR spectra of unweathered and weathered samples.

Table 3. Relative intensities of the FT-IR absorption peaks of samples.

Samples	Status	I ₁₇₃₀ / I ₁₄₅₃	I ₁₆₀₂ / I ₁₄₅₃	I ₁₄₉₃ / I ₁₄₅₃	I ₁₄₅₃ / I ₁₄₅₃	I ₁₃₈₂ / I ₁₄₅₃	I ₁₁₆₄ / I ₁₄₅₃	I ₁₁₁₈ / I ₁₄₅₃	I ₁₀₇₁ / I ₁₄₅₃	I ₉₉₁ / I ₁₄₅₃
CS	unweathered	0.99	0.58	0.73	1.00	0.69	0.94	0.83	0.64	0.50
	weathered	1.75	0.58	0.72	1.00	0.69	1.11	0.85	0.66	0.48
HC1	unweathered	1.02	0.58	0.72	1.00	0.70	0.96	0.85	0.66	0.51
	weathered	1.77	0.59	0.73	1.00	0.71	1.14	0.86	0.67	0.49
HC2	unweathered	1.04	0.58	0.73	1.00	0.69	0.96	0.84	0.65	0.51
	weathered	1.76	0.59	0.72	1.00	0.70	1.12	0.85	0.67	0.48
BZC	unweathered	1.23	0.58	0.73	1.00	0.68	0.99	0.82	0.64	0.48
	weathered	1.74	0.57	0.70	1.00	0.68	1.10	0.83	0.65	0.47
BZHC1	unweathered	1.43	0.57	0.74	1.00	0.68	1.04	0.82	0.63	0.48
	weathered	1.73	0.57	0.71	1.00	0.68	1.09	0.83	0.64	0.47
BZHC2	unweathered	1.31	0.57	0.74	1.00	0.68	1.01	0.82	0.63	0.48
	weathered	1.73	0.57	0.71	1.00	0.68	1.09	0.83	0.64	0.47

3.4. X-ray Photoelectron Spectroscopy Analysis

XPS analysis was used to determine the surface element species distribution of unweathered and weathered free films and the results are presented in Table S1. The C and O contents of the unweathered samples are distributed in the range of 60.14–67.44% and 32.56–39.86%, respectively. The O content of the samples showed an increasing trend after exposure, and a reverse trend was observed for the C content. The O/C ratio of samples showed varying degrees of growth (4.14–21.89; 5%) after 300 h of exposure. The O/C ratio of sample BZHC1 only increased by 4.14%, which is the smallest value among the six samples; this ratio increased by 5.03% and 6.09% for BZHC2 and BZC, respectively. A significant increase in the O/C ratio was observed for sample CS (21.89%), which was several times that of the O/C ratio of BZHC1 after weathering. The O/C ratios of samples HC1 and HC2 with added HALS showed obvious growth after exposure. These results confirm that the coating without protective materials is susceptible to solar radiation when exposed to outdoor conditions; the samples with added HALS are better at decreasing photodegradation, and the stereoscopic protective coatings with multicomponent protection significantly reduced photooxidation [50].

Figure S1 presents the C1s spectra of the unweathered and weathered samples, fitted into four peaks (C1, C2, C3, and C4); their energies and abundances are listed in Table S1. C1 is ascribed to C–C/C–H/C=C, with binding energies of 284.53–284.63 eV, while C2 is related to phenol, alcohol, or other C–O, with binding energies of 286.02–286.24 eV. C3 is attributed to carbonyl C=O (287.92–288.48 eV) and C4 is assigned to carboxyl or ester (O=C–O), with binding energies of 288.79–289.02 eV (Li et al., 2020). The proportions of C1 in the spectra of all samples declined after weathering. Conversely, the proportions of C2 and C4 in the six samples increased after 300 h of exposure. These results indicate that the samples underwent a series of photooxidation reactions. The smallest change in C content (−0.93%) (Table 3) was observed for sample BZHC1 which also exhibited the smallest decreases in C1 and C4 contents (−1.24% and −0.18%). The largest change in C content (−4.55%) was observed for sample CS; its decrease in C1 and C4 contents were −6.17% and −0.81%, respectively. The results suggest that sample BZHC1 has good stability when exposed to solar radiation. The C3 proportion of samples CS and HC2 increased after weathering, and reverse trends were observed for samples HC1, BZC, HZHC1, and BZHC2. This result for samples HC1, BZC, HZHC1, and BZHC2 is likely due to the greater transformation of C4 from C3 compared to the transformation of C3 from C1 and C2 in these samples during exposure, which also indicates that the transformation of C3 plays a leading role in photodegradation reactions [51].

The deconvolution of the O1s spectra of the unweathered and weathered samples is illustrated in Figure S2. The O1s peaks at 532.77–533.21 eV (O1) and 531.72–532.1 eV (O2) are attributed to O–C/chemisorbed oxygen and O=C/O=N, respectively. The proportions

of O1 in the spectra of all samples declined after 300 h of exposure, and a reverse tendency was observed for the proportions of O2. This result is consistent with previous results, clearly indicating that photooxidation occurs on the surface of all samples [51,52]. However, there were significant differences in the changes in O1 and O2 content between different samples. Sample CS presented the largest decrease in O1 (12.25%) and an increase in O2 (16.80%), followed by HC1, HC2, and BZC. The changes in the O2 contents of HC1 and HC2 were 10.18% and 7.15%, respectively, which were obviously less than those of sample CS and greater than that of sample BZC (6.24%). These results confirmed that the addition of HALS was effective in improving the photostability of free films. Much better O1 and O2 stabilities were observed in samples BZHC1 and BZHC2; the changes in O1 and O2 contents of BZHC1 were only -0.79% and 1.72% , respectively. These results were similar to those obtained by FT-IR spectroscopy [49].

3.5. Thermogravimetric Analysis of Free Films

TGA was performed to investigate the thermal decomposition and stability of free films by quantitatively measuring the weight loss over a specific temperature range [30]. The mass loss curves of the free films are shown in Figure 7, and the pyrolysis residual contents of various samples after treatment at $800\text{ }^{\circ}\text{C}$ are listed in Table 4. The whole thermogravimetric decomposition process can be divided into three stages. The first stage, within the $25\text{--}180\text{ }^{\circ}\text{C}$ temperature range, involves a slight loss of coating mass, which is mainly caused by the evaporation of adsorbed water in the sample. The second stage starts at around $200\text{ }^{\circ}\text{C}$ and ends at $420\text{ }^{\circ}\text{C}$; the weight of all samples dramatically decreased in this stage, indicating that this was the main pyrolysis temperature range of the free films. Mass changes in the samples were hardly observed when the pyrolysis temperature was in the $420\text{--}800\text{ }^{\circ}\text{C}$ range; this was considered as the third decomposition stage.

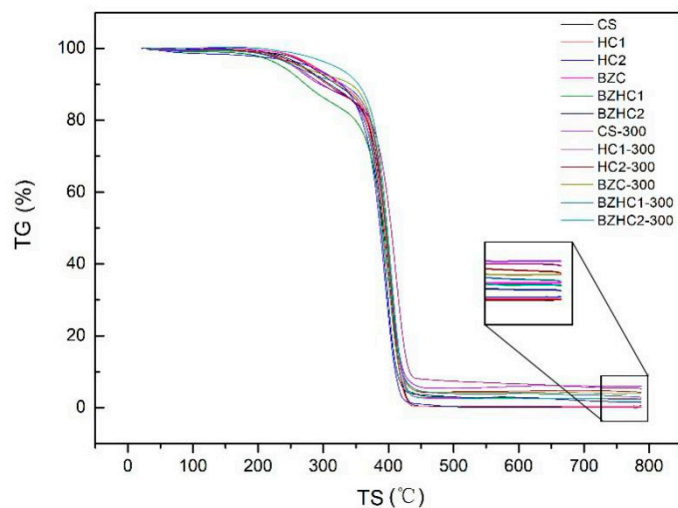


Figure 7. The TGA curves of unweathered and weathered samples.

Table 4. Pyrolysis residual content of unweathered and weathered samples.

	Pyrolysis Residual Content (%)					
	CS	HC1	HC2	BZC	BZHC1	BZHC2
Unweathered samples	0.07	0.16	0.52	2.60	2.18	1.41
Weathered samples	5.93	5.22	4.11	3.89	2.81	2.36
Changes	5.86	5.06	3.59	1.29	0.63	0.95

The unweathered CS samples were almost completely pyrolyzed when the treatment temperature was $800\text{ }^{\circ}\text{C}$, and the pyrolysis residue was 0.07% (CS). The pyrolysis residues

of the unweathered samples with added HA1 and HA2 increased to 0.16% (HC1) and 0.52% (HC2) compared to the unweathered CS samples, indicating that HALS contains structures that are not easily pyrolyzed. The pyrolysis residues of unweathered samples of BZC (2.60%), BZHC1 (2.18%), and BZHC2 (1.41%) were markedly increased compared with the unweathered samples of CS, HC1, and HC2, which was attributed to the addition of NZnO that is not pyrolyzed at 800 °C. The pyrolysis residue of weathered samples was greater than that of unweathered samples, suggesting that many components that were difficult to pyrolyze were produced during photodegradation [53]. The changes in the pyrolysis residues of the samples after weathering are listed in Table 4. The regular changes were similar to those in the above investigation. The largest change in the pyrolysis residue was obtained in sample CS (5.86%), followed by samples HC1 (5.06%) and HC2 (3.59%). The smallest change in pyrolysis residues was observed in sample BZHC1, suggesting that the stereoscopic protective coatings reduced the production of components that were not easily pyrolyzed, and increased the photostability of the coating when exposed to solar radiation [54].

HALS contains a large number of alicyclic amines. After absorbing light energy, HALS can combine with hydrogen in hydroperoxide and decompose into nitrogen and oxygen free radicals. These free radicals can intercept the active free radicals generated during photodegradation, reducing the sensitivity of the coating to UV radiation. At the same time, HALS can inhibit the photooxidation reaction between lignin and the binder in the coating and maintain the adhesion between the coating and the substrate, preventing the loss of gloss and transparency of the coating surface (Figure 8) [55,56].

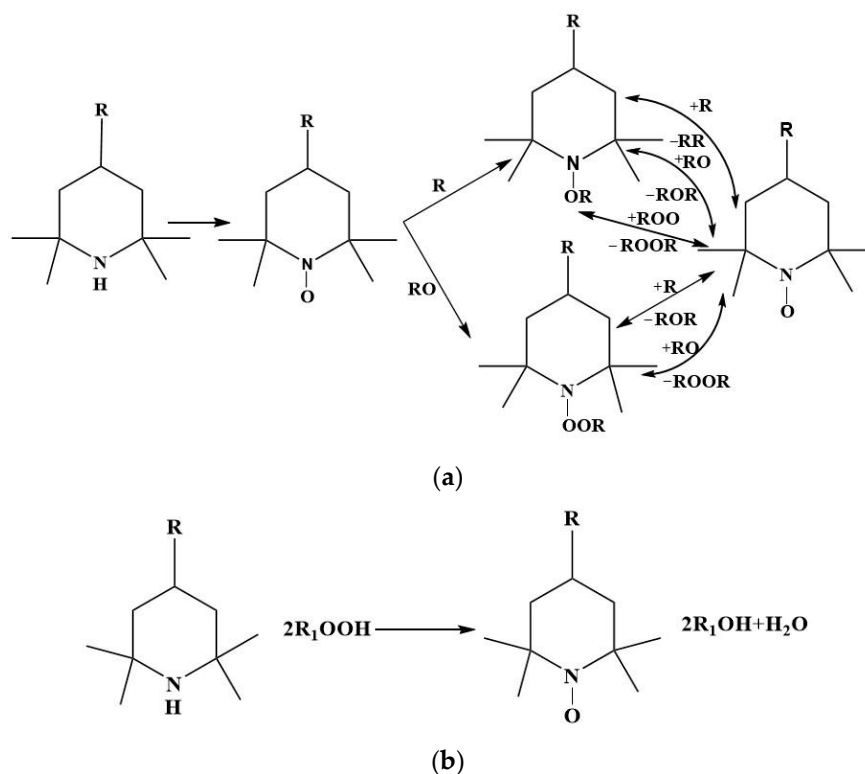


Figure 8. (a) The action mechanism of HALS capturing free radicals; (b) The mechanism of HALS in peroxide decomposition.

4. Conclusions

In summary, a stereoscopic protective coating containing a UV absorber and HALS was developed for the weathering protection of OBS. The surface properties and weathering behavior of free films and OBS were characterized. The samples had different degrees of photochemical reactions after weathering, especially for the CS samples without protection.

The stereoscopic protective coating of BZHC1 exhibited good improvement with the color photostability of OBS, and the ΔE^* value of sample BZHC1-B decreased by 76.67% compared with sample CS-B. This stereoscopic protective coating also enhanced the physical and chemical stability of the free film; the stability of C=O stretching, O/C ratio, C4, O2, and pyrolysis residues of sample BZHC1 increased by 72.67, 81.09%, 77.78%, 89.76%, and 89.25%, respectively, compared with sample CS. These results confirm that the coating containing UV absorbers and HALS was superior for the protection of OBS and the coating itself. This study proposes an effective anti-weathering protection scheme for bamboo and wood products, which in turn, can help conserve forest resources.

Supplementary Materials: The following supporting information can be downloaded at: <https://www.mdpi.com/article/10.3390/f13030467/s1>, Figure S1: C1s XPS spectra of unweathered and weathered free films; Figure S2: O1s XPS spectra of unweathered and weathered free film; Table S1: XPS data of unweathered and weathered free film.

Author Contributions: Conceptualization, Y.Y. and L.Z.; methodology, H.H.; validation, M.B.; formal analysis, Z.W.; investigation, Y.B. and Y.Y.; resources, N.L. and Z.Z.; data curation, L.Z. and H.H.; writing—original draft preparation, Y.Y. and L.Z.; writing—review and editing, Y.Y. and L.Z.; visualization, Z.W.; supervision, Y.B.; project administration, Y.C.; funding acquisition, N.L. and Z.Z. All authors have read and agreed to the published version of the manuscript.

Funding: This research was funded by the Fundamental Research Funds for the Central Non-profit Research Institution of CAF (CAFYBB2021ZX001-02) (N.L.), National Natural Science Foundation of China (31872697) (Z.Z.), 2021 Provincial Science and Technology Innovation Leading Talents (2021RC4033) (Z.Z.) and Young Scholars Training Program (2020TJ-Q18) (Z.Z.).

Data Availability Statement: The datasets generated during and/or analyzed during the current study are available from the corresponding author on reasonable request.

Conflicts of Interest: The authors declare no conflict of interest.

References

1. Li, Z.; Chen, C.; Mi, R.; Gan, W.; Dai, J.; Jiao, M.; Xie, H.; Yao, Y.; Xiao, S.; Hu, L. A Strong, Tough, and Scalable Structural Material from Fast-growing Bamboo. *Adv. Mater.* **2020**, *32*, 1906308. [\[CrossRef\]](#)
2. Nkeuwa, W.; Zhang, J.; Semple, K.; Chen, M.; Xia, Y.; Dai, C. Bamboo-based composites: A review on fundamentals and processes of bamboo bonding. *Compos. Part B Eng.* **2022**, *235*, 109776. [\[CrossRef\]](#)
3. Wang, Y.; Wang, X.; Li, Y.; Huang, P.; Yang, B.; Hu, N.; Fu, S. High-Performance Bamboo Steel Derived from Natural Bamboo. *ACS Appl. Mater. Interfaces* **2020**, *13*, 1431–1440. [\[CrossRef\]](#) [\[PubMed\]](#)
4. Vorontsova, M.S.; Clark, L.G.; Dransfield, J.; Govaerts, R.; Baker, W.J. *World Checklist of Bamboos and Rattans*; Science Press: Beijing, China, 2017; Volume 1.
5. Müller, U.; Rätzsch, M.; Schwanninger, M.; Steiner, M.; Zöbl, H. Yellowing and IR-changes of spruce wood as result of UV-irradiation. *J. Photochem. Photobiol. B Biol.* **2003**, *69*, 97–105. [\[CrossRef\]](#)
6. Kanbayashi, T.; Kataoka, Y.; Ishikawa, A.; Matsunaga, M.; Kobayashi, M.; Kiguchi, M. Confocal Raman Microscopy Reveals Changes in Chemical Composition of Wood Surfaces Exposed to Artificial Weathering. *J. Photochem. Photobiol. B* **2018**, *187*, 136–140. [\[CrossRef\]](#) [\[PubMed\]](#)
7. Kim, Y.S.; Lee, K.H.; Kim, J.S. Weathering characteristics of bamboo (*Phyllostachys puberescence*) exposed to outdoors for one year. *J. Wood Sci.* **2016**, *62*, 332–338. [\[CrossRef\]](#)
8. Evans, P.; Chowdhury, M.J.; Mathews, B.; Schmalzl, K.; Ayer, S.; Kiguchi, M.; Kataoka, Y. Weathering and surface protection of wood. In *Handbook of Environmental Degradation of Materials*; William Andrew: Norwich, NY, USA, 2005; pp. 277–297.
9. Evans, P.D.; Gibson, S.K.; Cullis, I.; Liu, C.; Sèbe, G. Photostabilization of wood using low molecular weight phenol formaldehyde resin and hindered amine light stabilizer. *Polym. Degrad. Stab.* **2013**, *98*, 158–168. [\[CrossRef\]](#)
10. Czajkowski, W.; Mammnicka, J.; Lota, W.; Lewartowska, J. Application of reactive UV-absorbers for increasing protective properties of cellulose fabrics during standard laundering process. *Fibers Polym.* **2012**, *13*, 948–953. [\[CrossRef\]](#)
11. Homan, W.J.; Jorissen, A.J.M. Wood Modification Developments. *Heron* **2004**, *49*, 361–386.
12. Hill, C.; Altgen, M.; Rautkari, L. Thermal Modification of Wood—A Review: Chemical Changes and Hygroscopicity. *J. Mater. Sci.* **2021**, *56*, 6581–6614. [\[CrossRef\]](#)
13. Jirouš-Rajković, V.; Miklečić, J. Heat-Treated Wood as a Substrate for Coatings, Weathering of Heat-Treated Wood, and Coating Performance on Heat-Treated Wood. *Adv. Mater. Sci. Eng.* **2019**, *2019*, 8621486. [\[CrossRef\]](#)
14. Kamperidou, V.; Barboutis, I. Natural Weathering performance of thermally treated poplar and black pine wood. *Maderas Cienc. Y Tecnol.* **2021**, *23*, 1–21. [\[CrossRef\]](#)

15. Hill, C.A.S. *Wood Modification: Chemical, Thermal and Other Processes*; Wiley Series in Renewable Resources; John Wiley & Sons: Chichester, UK; Hoboken, NJ, USA, 2006; ISBN 978-0-470-02172-9.
16. Rowell, R.M. Chemical modification of wood. In *Handbook of Wood Chemistry and Wood Composites*; Rowell, R.M., Ed.; CRC Press: Boca Raton, FL, USA, 2005; ISBN 978-0-8493-1588-6.
17. Chang, H.-T.; Chang, S.-T. Modification of Wood with Isopropyl Glycidyl Ether and Its Effects on Decay Resistance and Light Stability. *Bioresour. Technol.* **2006**, *97*, 1265–1271. [[CrossRef](#)]
18. Rowell, R.M. Acetylation of Wood—Journey from Analytical Technique to Commercial Reality. *For. Prod. J.* **2006**, *56*, 4–12.
19. Evans, P.D.; Wallis, A.F.A.; Owen, N.L. Weathering of Chemically Modified Wood Surfaces. *Wood Sci. Technol.* **2000**, *34*, 151–165. [[CrossRef](#)]
20. Kalnins, M.A. Photochemical Degradation of Acetylated, Methylated, Phenylhydrazine-Modified, and ACC-Treated Wood. *J. Appl. Polym. Sci.* **1984**, *29*, 105–115. [[CrossRef](#)]
21. Beckers, E.P.J.; Meijer, M.; Militz, H.; Stevens, M. Performance of Finishes on Wood That Is Chemically Modified by Acetylation. *J. Coat. Technol.* **1998**, *70*, 59–67. [[CrossRef](#)]
22. Bongers, F.; Creemers, J.; Kattenbroek, B.; Homan, W. Performance of Coatings on Acetylated Scots Pine after More than Nine Years Outdoor Exposure. In *Proceedings of the Wood Modification: Processes, Properties and Commercialisation*, Göttingen, Germany, 6–7 October 2005; Militz, H., Hill, C., Eds.; ECWM: Spring, MD, USA, 2005; pp. 125–129.
23. Cristea, M.V.; Riedl, B.; Blanchet, P. Enhancing the performance of exterior waterborne coatings for wood by inorganic nanosized UV absorbers. *Prog. Org. Coat.* **2010**, *69*, 432–441. [[CrossRef](#)]
24. Muasher, M.; Sain, M. The efficacy of photostabilizers on the color change of wood filled plastic composites. *Polym. Degrad. Stab.* **2006**, *91*, 1156–1165. [[CrossRef](#)]
25. Boisvert, J.P.; Persello, J.; Castaing, J.C.; Cabane, B. Dispersion of alumina-coated TiO₂ particles by adsorption of sodium polyacrylate. *Colloids Surf. A Physicochem. Eng. Asp.* **2001**, *178*, 187–198. [[CrossRef](#)]
26. Liufu, S.C.; Xiao, H.N.; Li, Y.P. Thermal analysis and degradation mechanism of polyacrylate/ZnO nanocomposites. *Polym. Degrad. Stab.* **2005**, *87*, 103–110. [[CrossRef](#)]
27. Yu, Y.; Jiang, Z.; Wang, G.; Tian, G.; Wang, H.; Song, Y. Surface functionalization of bamboo with nanostructured ZnO. *Wood Sci. Technol.* **2012**, *46*, 781–790. [[CrossRef](#)]
28. Choi, S.S.; Chung, H.S. Novel co-matrix systems for the MALDI-MS analysis of polystyrene using a UV absorber and stabilizer. *Analyst* **2013**, *138*, 1256–1261. [[CrossRef](#)] [[PubMed](#)]
29. Rao, F.; Chen, Y.H.; Zhao, X.P.; Cai, H.J.; Li, N. Enhancement of bamboo surface photostability by application of clear coatings containing a combination of organic/inorganic UV absorbers. *Prog. Org. Coat.* **2018**, *124*, 314–320. [[CrossRef](#)]
30. Li, N.; Bao, M.; Rao FShu, Y.; Huang, C.; Huang, Z.; Chen, Y.; Bao, Y.; Guo, R.; Xiu, C. Improvement of surface photostability of bamboo scrimber by application of organic UV absorber coatings. *J. Wood Sci.* **2019**, *65*, 1–9. [[CrossRef](#)]
31. Li, N.; Chen, Y.; Yu, H.; Xiong, F.; Yu, W.; Bao, M.; Wu, Z.; Huang, C.; Rao, F.; Li, J.; et al. Evaluation of optical properties and chemical structure changes in enzymatic hydrolysis lignin during heat treatment. *RSC Adv.* **2017**, *7*, 20760–20765. [[CrossRef](#)]
32. Rajan, V.V.; WäBer, R.; Wieser, J. Influence of different types of UV absorber/UV stabilizer combination on the photodegradation of PC/ABS blend. *J. Appl. Polym. Sci.* **2012**, *124*, 4007–4015. [[CrossRef](#)]
33. Li, N.; Chen, Y.; Bao, Y.; Zhang, Z.; Wu, Z.; Chen, Z. Evaluation of UV-permeability and photo-oxidisability of organic ultraviolet radiation-absorbing coatings. *Appl. Surf. Sci.* **2015**, *332*, 186–191. [[CrossRef](#)]
34. Oberhofnerová, E.; Imnková, K.; Dvoák, O.; Štěrbová, I.; Hiziroglu, S.; Šedivka, P.; Pánek, M. Comparison of Exterior Coatings Applied to Oak Wood as a Function of Natural and Artificial Weathering Exposure. *Coatings* **2019**, *9*, 864. [[CrossRef](#)]
35. Rao, F.; Zhang, Y.; Bao, M.; Zhang, Z.; Bao, Y.; Li, N.; Chen, Y.; Yu, W. Photostabilizing Efficiency of Acrylic-based Bamboo Exterior Coatings Combining Benzotriazole and Zinc Oxide Nanoparticles. *Coatings* **2019**, *9*, 533. [[CrossRef](#)]
36. *ASTM G154-16*; Standard Practice for Operating Fluorescent Ultraviolet (UV) Lamp Apparatus for Exposure of Nonmetallic Materials. ASTM: West Conshohocken, PA, USA, 2016.
37. *ASTM D2244-07*; Standard Practice for Calculation of Color Tolerances and Color Differences from Instrumentally Measured Color Coordinates. ASTM: West Conshohocken, PA, USA, 2005.
38. Jämsä, S.; Ahola, P.; Viitaniemi, P. Long-term Natural Weathering of Coated Thermo Wood. *Pigment. Resin Technol.* **2000**, *29*, 68–74. [[CrossRef](#)]
39. Paulsson, M.; Parkas, J. Review: Light-induced yellowing of lignocellulosic pulps—Mechanisms and preventive methods. *BioResources* **2012**, *7*, 5995–6040. [[CrossRef](#)]
40. Feist, W.C.; Hon, D.N.-S. Chemistry of weathering and protection. In *The Chemistry of Solid Wood*; Advances in Chemistry Series; Rowell, R.M., Ed.; American Chemical Society: Washington, DC, USA, 1984; pp. 401–451. ISBN 978-0-8412-0796-7.
41. Pandey, K.K. Study of the Effect of Photo-Irradiation on the Surface Chemistry of Wood. *Polym. Degrad. Stab.* **2005**, *90*, 9–20. [[CrossRef](#)]
42. George, B.; Suttie, E.; Merlin, A.; Deglise, X. Photodegradation and Photostabilisation of Wood—The State of the Art. *Polym. Degrad. Stab.* **2005**, *88*, 268–274. [[CrossRef](#)]
43. Forsthuber, B.; Schaller, C.; Gruell, G. Evaluation of the photo stabilising efficiency of clear coatings comprising organic UV absorbers and mineral UV screeners on wood surfaces. *Wood Sci. Technol.* **2013**, *47*, 281–297. [[CrossRef](#)]

44. Leng, Y.; Xu, Q.; Liu, K. Experimental study on anti-aging performance of engineered bamboo for structural use under UV radiation. *Build. Struct.* **2021**, *51*, 131–134.
45. Forsthuber, B.; Gruell, G. The effects of HALS in the prevention of photo-degradation of acrylic clear topcoats and wooden surfaces. *Polym. Degrad. Stab.* **2010**, *95*, 746–755. [[CrossRef](#)]
46. Hayoz, P.; Peter, W.; Rogez, D. A New Innovative Stabilization Method for the Protection of Natural Wood. *Prog. Org. Coat.* **2003**, *48*, 297–309. [[CrossRef](#)]
47. Neumann, M.G.; Machado, A.E.H. The role of oxygen in the photodegradation of lignin in solution. *J. Photochem. Photobiol. B Biol.* **1989**, *3*, 473–481. [[CrossRef](#)]
48. Chiantore, O.; Trossarelli, L.; Lazzari, M. Photooxidative degradation of acrylic and methacrylic polymers. *Polymer* **2000**, *41*, 1657–1668. [[CrossRef](#)]
49. Chang, C.W.; Lee, J.J.; Lu, K.T. The Effects of Adding Different HALS on the Curing Process, Film Properties and Lightfastness of Refined Oriental Lacquer. *Polymers* **2020**, *12*, 990. [[CrossRef](#)] [[PubMed](#)]
50. Liu, Z.; Chen, S.; Zhang, J. Effect of UV absorbers and hindered amine light stabilizers on the photodegradation of ethylene–octene copolymer. *J. Appl. Polym. Sci.* **2012**, *127*, 1135–1147. [[CrossRef](#)]
51. Rao, F.; Ji, Y.; Yang, Y.; Zhang, Y.; Li, N.; Yu, W.; Chen, Y. Rapid Process Natural Bamboo into Outdoor Bamboo-Fiber-Reinforced Composite with High Surface Photostability. *Forests* **2021**, *12*, 446. [[CrossRef](#)]
52. Schaller, C.; Rogez, D.; Braig, A. Hydroxyphenyl-s-Triazines: Advanced Multipurpose UV-Absorbers for Coatings. *J. Coat. Technol. Res.* **2008**, *5*, 25–31. [[CrossRef](#)]
53. Queant, C.; Blanchet, P.; Landry, V.; Schorr, D. Effect of Adding UV Absorbers Embedded in Carbonate Calcium Templates Covered with Light Responsive Polymer into a Clear Wood Coating. *Coatings* **2018**, *8*, 265. [[CrossRef](#)]
54. Lowry, M.S.; Hubble, D.R.; Wressell, A.L.; Vratsanos, M.S.; Pepe, F.R.; Hegedus, C.R. Assessment of UV-Permeability in Nano-ZnO Filled Coatings via High Throughput Experimentation. *J. Coat. Technol. Res.* **2008**, *5*, 233–239. [[CrossRef](#)]
55. Gryn’Ova, G.; Ingold, K.U.; Coote, M.L. New insights into the mechanism of amine/nitroxide cycling during the hindered amine light stabilizer inhibited oxidative degradation of polymers. *J. Am. Chem. Soc.* **2012**, *134*, 12979–12988. [[CrossRef](#)] [[PubMed](#)]
56. Sinohara Souza, P.M.; Morales, A.R.; Saraiva Sanchez, E.M.; Innocentini Mei, L.H. Study of PBAT Photostabilization with Ultraviolet Absorber in Combination with Hindered Amine Light Stabilizer and Vitamin E, Aiming Mulching Film Application. *J. Polym. Environ.* **2018**, *26*, 1–15.